Method for efficient shape parametrization of fluid membranes and vesicles

Malcolm I. G. Bloor and Michael J. Wilson
Department of Applied Mathematics, The University of Leeds, Leeds LS2 9JT, United Kingdom
(Received 27 October 1999)

In this paper we describe a method for the parametrization of the shapes adopted by fluid membranes and vesicles. The method is based upon a boundary-value approach to geometry description in which smooth surfaces are produced as the solution to an elliptic partial differential equations. Shape parameters are introduced through the boundary conditions, which control the shape of the vesicle models. In combination with a model for the surface energy and a method for numerical minimization, it is shown how the method can accurately approximate the shapes of both axisymmetric and nonaxisymmetric vesicles over a wide range of control parameters. The particular value of the method lies in its ability to parametrize complicated shapes efficiently, a feature that becomes especially valuable when seeking shapes of minimal energy using direct optimization techniques.

PACS number(s): 87.10.+e, 87.16.Ac, 87.16.Dg

I. INTRODUCTION

A lipid molecule typically consists of a polar hydrophilic head and an hydrophobic tail consisting of hydrocarbon chains. Such amiphiphilic molecules when placed in aqueous solution can spontaneously aggregate to form encapsulating bags called vesicles. The membrane forming the walls of the vesicle consists of two monomolecular layers held together by weak noncovalent forces, where the lipid molecules orient themselves so that the hydrophilic heads are turned outwards towards the surrounding aqueous environment whilst the hydrophobic tails are turned inwards. This structural arrangement of the molecules forming the membrane is usually referred to as a bilayer, and by organizing themselves in this way the lipid molecules greatly reduce the surface energy of the membrane. Even though a membrane is typically only a few nanometers thick, the vesicles themselves can be of macroscopic proportions of up to 100 μm [1].

In fact, depending upon the chemical and physical properties of their molecules, as well as that of their environment, amphiphilic compounds can assemble into a wide range of different types of aggregates: spherical micelles, elongated micelles, branched micelles, flat or discoidal miscelles, ribbons, etc., as well as bilayers [2]. However, bilayers have received a great deal of study in recent years, since this type of membrane is the fundamental structural component of the boundaries of all cells and cell organelles. Consequently behavior of vesicles composed of lipid bilayers under the influence of different chemical and physical environments has been used as a simplified model for the behavior of cells.

Despite the relatively simple structure of their walls, vesicles can adopt a wide variety of different shapes and even topologies [1]. Theoretical explanations for the configurations adopted by vesicles have tended to follow a continuum model in which the dominant effect is the bending elasticity of the membrane, in contrast to other types of fluid interfaces where surface tension plays the primary role. The first such models were put forward in the 1970s (Canham [3], Helfrich [4], Evans [5]), and although refinements have been put forward since—see, for example, Svetina *et al.* [6], Seifert *et al.* [7], or the comprehensive review of Seifert [1]—all assume that vesicles acquire the shape for which their surface energy is minimal (in a local sense at least), subject to appropriate constraints. As far as these models are concerned, on the length scales of the vesicles the properties of the lipid molecules are important only insofar as they determine the various elastic constants of the continuum energy model; although whether or not a bilayer is formed in the first place, as opposed to micelles, for example, is dependent on the structure of the lipid molecules [1]. It is also commonly assumed that nonequilibrium effects and thermal fluctuations can be neglected except near shape transitions [1]. Where the various models differ is in their estimate of the functional relationship between the energy of the surface and its shape. In a review, Seifert [1] gives a detailed summary of the various theoretical models, but their main features may be summarized briefly as follows.

In 1970 Canham [3], seeking to explain the shape of erythrocytes, suggested that the local energy density of the membrane was proportional to the sum of the squares of the principal curvatures, a model which is appropriate for a vesicle consisting of a symmetric bilayer. Helfrich [4] subsequently modified this model and introduced the so-called spontaneous curvature C_0 to reflect a possible asymmetry between the two layers of the membrane. Such an asymmetry could arise because of different environments on either side of the membrane, or else because of differences in the chemical composition between the two monolayers. The energy functional for the surface is given in Eq. (7). According to this model, the shape adopted by a vesicle is such as to locally minimize the energy functional subject to the constraints of constant area and volume.

In some ways similar to the spontaneous curvature (SC) model is the bilayer couple model ([6,8,9]) in which there is an additional constraint on the integrated mean curvature of the membrane, which turns out to have the effect of making the spontaneous curvature unimportant [1]. The model is based on the assumption that each layer of the bilayer is incompressible but can be bent, and therefore can store elastic energy. Finally there is the area-difference-elasticity (ADE) model (Seifert *et al.*, [7], Wiese *et al.* [10], Bozic *et al.* [11]) in which the energy functional for a membrane

contains a local contribution from the curvature energy and a nonlocal contribution from the deviation in the area difference between the two monolayers from a reference value. In the ADE model the energy functional is minimized subject to constraints upon the area and volume.

When it comes to calculating the shapes of vesicles there are, broadly speaking, three categories of method used to calculate the shapes of vesicles: (a) solving the Euler-Lagrange equations associated with the integral expression for the total surface energy; (b) using a parametrized model for the shape of a vesicle and then choosing the values of the various parameters in the model so as to obtain the shape with lowest energy; and (c) ''brute-force'' minimization of the surface energy of a triangulated surface model of the vesicle.

As noted by Seifert [1], most work has been done in the context of the first approach, where the Euler-Lagrange equations yields a set of solutions for which the first variation of the appropriate functional, combining both the energy of the surface and imposed constraints, vanishes. These stationary solutions correspond either to locally stable shapes or saddle points (which can be identified by stability analysis). Seifert [1] reviews this approach and in particular considers the derivation of the appropriate Euler-Lagrange equation which is a fourth-order nonlinear partial differential equation (originally derived by Ou-Yang and Helfrich [12]). The solution of this equation in full generality is a formidable task and has not yet been achieved, hence most work has concentrated upon the solution of the axisymmetric case, where the Euler-Lagrange equation is a nonlinear ordinary differential equation. The usual approach to obtaining and solving this equation is to substitute a parametrization of an axisymmetric shape into the energy functional, and a number of parametrizations have been considered in the context of various energy models, e.g., Helfrich [4], Svetina and Zeks [9], Miao *et al.* [13], and Seifert *et al.* [14].

The second approach, that of approximating a vesicle's shape using a parametrized model with a restricted parameter set, and then choosing the parameters in order to minimize the surface energy, is sometimes referred to as the variational approach. An example of this type of method can be found in the work of Canham [3], who used Cassini ovals to parametrize the shape of red blood cells; another example is the work of Heinrich *et al.* [15] who used spherical harmonics to parametrize the vesicles.

The third approach is that of minimizing the curvature energy of a triangulated surface model. The parameters in this model are in effect the positions of the vertices of the surface triangles, of which there can be a large number and in consequence the computational cost of numerically minimizing the surface energy can be enormous. However, this approach has been employed successfully by a number of workers to find nonaxisymmetric shapes, e.g., Refs. [16–18].

The approach to predicting vesicle shape adopted in this paper falls into the category of using a parametrized surface model to represent the vesicle surface and then choosing the values of various ''shape'' parameters introduced in the model so as to obtain the surface of lowest energy subject to appropriate constraints. This method for surface parametrization was developed in the context of industrial computer-aided design (CAD), where the problem is to devise mathematical methods with which to describe the geometry of objects with complex ''freeform'' shapes such as aircraft, ships, engine components, etc., with a view to computer-based design, analysis, and optimization of the objects before they are eventually manufactured. In CAD there is a trend towards ''simulation-based design,'' where many of the changes to a design are made as the result of computer analysis of the appropriate physics, and are made automatically using the methodology of numerical optimization. There is, therefore, a requirement for a method for shape representation that can parametrize efficiently complex shapes, in the sense of requiring only a limited set of design variables.

The method for shape parametrization is described in detail in Sec. II, but basically it adopts a boundary-value approach to shape generation, and produces a description of an object's surface shape as a mapping from a simple space to a complex surface embedded in 3-space. The mapping is achieved by solving an elliptic partial differential equation [19], unlike conventional methods for surface description in CAD which are based on polynomial splines [20]. For the sake of example, the method is presented in the context of the spontaneous curvature (SC) model of Helfrich [4], where it is used in combination with a method for numerical optimization to find the shape of vesicles not only qualitatively but also quantitatively, The purpose of this paper is to describe the method rather than to undertake any systematic investigation of vesicle shapes for a particular energy model. However, the method is validated by producing phase diagrams for various test cases that can be compared with the earlier work of others, e.g., [14].

Section III describes a simple model of a vesicle shape produced from a single surface patch, which is capable of producing both axisymmetric oblate and prolate shapes. Results are presented which show how the surface energy of both the prolate and oblate branches vary as a function of reduced volume. In Sec. IV the model is refined by using two surface patches to represent the shape of a vesicle. Again in the case of zero spontaneous curvature it is demonstrated how the surface parametrization is capable of reproducing not only the oblate and prolate branches but now the stomatocyte branch of the phase diagram. As a further test of the model, the phase diagram for a nonzero value of the spontaneous curvature is calculated. Finally, in Sec. V, the surface model is used to calculate some nonaxisymmetric shapes for both the SC model and the area-difference-elasticity (ADE) model.

II. METHOD FOR SHAPE PARAMETRIZATION

In the context of industrial CAD the method for shape parametrization presented in this paper is referred to as the partial differential equation (PDE) method. As mentioned in Sec. I, the method views surface generation as a boundary-value problem and it generates surfaces as mappings from the solutions of elliptic partial differential equations. What this means in geometric terms is that a surface patch is generated from data specified around its edges, the data typically taking the form of a mathematical parametrization of the curves around the edges of the patch, along with derivative information which controls how the surface patch meets the edge curves. By a suitable choice of boundary conditions the method is able to generate a wide variety of object shapes.

In mathematical terms, a PDE surface is found in as a function $\underline{X}(u,v)$ which is the solution to a boundary-value problem formulated in parameter space. More specifically, we introduce two scalar variables u and v as the coordinates of a point in a region Ω of a two-dimensional parameter space, and the function $\underline{X}(u,v)$ as a mapping from Ω to a patch of surface in Euclidean 3-space, where $\underline{X}(u,v)$ satisfies boundary conditions imposed on $\partial\Omega$. To satisfy these requirements we regard $\underline{X}(u,v)$ as the solution of a partial differential equation of the general form

$$D^m_{uv}(\underline{X})=\underline{F}(u,v), \tag{1}$$

where $D^m_{uv}()$ is a partial differential operator of order m in the independent variables u and v, while $\underline{F}(u,v)$ is a vector function of u and v. Since we are adopting a boundary-value approach, it is natural to consider the class of elliptic partial differential equations. The elliptic PDE acts as an averaging operator and produces the surface patch as a smooth transition between the boundary conditions. In contrast, in conventional CAD systems, the mapping effected by Eq. (1) is achieved by expressing the function $\underline{X}(u,v)$ a finite sum of polynomial basis functions, so that a surface is controlled by a net or polygon of ''control'' points distributed around the surface in 3-space. However, because the data required to specify a PDE surface is specified around its edges, rather than across its surface, a much smaller number of shape parameters are needed to describe a complex surface using the PDE methodology. So, for example, in the case of a complex object such as a swirl inlet-port for a diesel engine, about 50 shape parameters are needed, whereas for a conventional CAD system many hundreds if not thousands of control points are required [21].

In CAD one is often seeking to generate surface patches that meet neighboring surfaces with a specified degree of continuity. Since the level of continuity is often confined to continuity of tangent plane, most work using the PDE method in CAD has been done using a fourth-order elliptic equation. Even so, just by the specifying the function and its first derivative at the boundaries, shapes of considerable complexity have been produced, e.g., [21]. If curvature continuity across patch boundaries is required in addition, then a sixth-order equation must be solved, and since curvature continuity is a requirement for the surface descriptions used in this paper, vesicle shapes are generated from solutions to the following sixth-order elliptic partial differential equation:

$$\left(\frac{\partial^2}{\partial u^2}+a^2\frac{\partial^2}{\partial v^2}\right)^3\underline{X}=0, \tag{2}$$

which is solved independently for the x, y, and z components of points on the surface.

The partial differential operator in Eq. (2) represents a smoothing process in which the value of the function at any point on the surface is, in a sense, an average of the surrounding values. In this way a surface is obtained as a smooth transition between the boundary conditions imposed on the function and its parametric derivatives. The parameter a, which we will refer to as the smoothing parameter, controls the relative rates of smoothing between the u and v parameter directions.

Although the justification for using this equation in the present application is ultimately its usefulness, some words of explanation for the choice of Eq. (2) are in order. Equation (2) is not chosen as being in some way a linearized approximation to the shape equations. In the present situation, where vesicle shapes will be constructed by joining more than one patch of PDE surface together, and where the surface energy is a function of curvature, one would like a surface description where the curvature is continuous across patch boundaries. Hence the boundary conditions used to solve the generating PDE need to specify not only the function $\underline{X}$ but also its first and second parametric derivatives, which is the reason why Eq. (2) is sixth order. Furthermore, the boundary conditions are the means by which the surface shape can be controlled, and the more derivatives one can specify the greater the control one can exercise over the shape, even within the constraints set by continuity conditions at the boundaries. Here, being able to specify the second derivative as well, gives an even degree of control.

From a solution to Eq. (2) a generic parameteric model of a vesicle shape can be constructed which is capable of producing a wide range of possible geometries. The model contains a number of ''shape'' parameters that are introduced through the boundary conditions (see below). The values of the shape parameters determine the specific geometry of the vesicle, and in this paper the values of the shape parameters are selected to give a surface with minimum energy. The parametrization can be made hierarchical in the sense that at first, only parameters that produce large-scale features of the shape are introduced; then, later, the geometry model can be refined, and additional shape parameters introduced, to capture finer detail in the shape. In this way the computational cost of numerical optimization can be reduced. This approach has been used in Sec. V where nonaxisymmetric vesicle shapes are considered, and in the CAD area, a hierarchical approach has been used to design wings [22].

Finally, Eq. (2) has the advantage that the surfaces produced are quick and easy to generate. They respond in an intuitive fashion to changes in the boundary conditions and can be manipulated in ''real-time'' by a user sitting at a workstation or PC. The relevant physical characteristics of the object in question can be calculated from the surface description using software for the specific analysis, and the surface can be quickly changed in order to optimize the desired properties. Thus, even though the parametrizations of vesicle shapes described in this paper are approximations to the actual shape in a particular situation, the approximations are accurate, surprisingly so given the small number of patches actually used.

To find a solution to Eq. (2) we can specify along $\partial\Omega$ boundary conditions on the function $\underline{X}$ and its first and second (parametric) derivatives in a direction normal to the boundary $\partial\Omega$ in parameter space. The parametrizations considered in this work are periodic in one of the parameter directions, which we shall take to be the v direction, and in the discussion that follows we will consider solutions over the (u,v) region $[0,1]\times[0,2\pi]$. Restricting the discussion to such surfaces does not unduly reduce the range of surface shapes that we can generate and, furthermore, a very fast method for generating such surfaces can be used. Thus, the boundary conditions used to solve Eq. (2) are of the form

$$\underline{X}(0,v)=\underline{f}^0(v), \tag{3a}$$

$$\underline{X}(1,v)=\underline{f}^1(v), \tag{3b}$$

$$\underline{X}_u(0,v)=\underline{f}^0_u(v), \tag{3c}$$

$$\underline{X}_u(1,v)=\underline{f}^1_u(v), \tag{3d}$$

$$\underline{X}_{uu}(0,v)=\underline{f}^0_{uu}(v), \tag{3e}$$

$$\underline{X}_{uu}(1,v)=\underline{f}^1_{uu}(v). \tag{3f}$$

The boundary conditions $\underline{f}^0(v)$ and $\underline{f}^1(v)$ give the two curves that form the edges of the surface patch in terms of the periodic variable v; the boundary conditions on the first parametric derivatives $\underline{f}^0_u(v)$ and $\underline{f}^1_u(v)$ determine the ''speed'' and direction in which the surface leaves the edge curves (and hence the direction of the surface normal at the edges of the patch), whilst the boundary conditions on the second parametric derivatives $\underline{f}^0_{uu}(v)$ and $\underline{f}^1_{uu}(v)$ control the surface curvature at the edges of the patch. Note that the shape parameters that control the surface are introduced through the boundary conditions (see below).

For periodic boundary conditions which can be represented by a finite Fourier decomposition, we can write down the solution to Eq. (2) in closed-form, thus

$$\underline{X}(u,v)=\underline{A}_0(u)+\sum_{n=1}^{M}\{\underline{A}_n(u)\cos(nv)+\underline{B}_n(u)\sin(nv)\}. \tag{4}$$

Note that in more general situations a solution can be found using a pseudospectral method [23]. The functions $\underline{A}_n(u)$ and $\underline{B}_n(u)$ are of the form

$$\underline{A}_0(u)=\underline{a}_{00}+\underline{a}_{01}u+\underline{a}_{02}u^2+\underline{a}_{03}u^3, \tag{5a}$$

$$\underline{A}_n(u)=\underline{a}_{n0}e^{anu}+\underline{a}_{n1}e^{-anu}+\underline{a}_{n2}ue^{anu}+\underline{a}_{n3}ue^{-anu}+\underline{a}_{n4}u^2e^{anu}+\underline{a}_{n5}u^2e^{-anu}, \tag{5b}$$

$$\underline{B}_n(u)=\underline{b}_{n0}e^{anu}+\underline{b}_{n1}e^{-anu}+\underline{b}_{n2}ue^{anu}+\underline{b}_{n3}ue^{-anu}+\underline{b}_{n4}u^2e^{anu}+\underline{b}_{n5}u^2e^{-anu}. \tag{5c}$$

The constant vectors $\underline{a}_{n0}, \underline{b}_{n0}$, etc., are determined by the boundary conditions. Note that there is a further parameter used to control the shape and this is the smoothing parameter a that occurs in the governing partial differential equation [Eq. (2)]. By adjusting the value of a one can change the properties of the surface, either propagating the effects of the boundary conditions over substantial parts of the surface, or confining their effects to regions near the edges of the surface. For large a, changes in the u direction occur over a relatively short length scale, namely $1/a$ times the length scale in the v direction over which similar changes take place. Note that it is possible to associate different values of a with features on the surface of different length scales, although at the cost of adding additional parameters to the problem.

By a suitable choice of boundary conditions, and by joining together more than one surface patch, a wide range of surface shapes can be created. For example, work in the area of industrial design has shown how the method can efficiently parametrize the surface of such objects as aircraft [24], ships [25], propellers, and engine components [21]. Note that the boundary conditions have an intuitive geometric interpretation, and in fact software has been written that enables a designer, knowing nothing of the underlying mathematics, to design complicated shapes at a workstation or PC. In the present application the choice of shape parameters is made on the basis of minimizing the surface energy of the vesicle subject to suitable constraints, a process which is carred out automatically using an algorithm for numerical optimization described in more detail below.

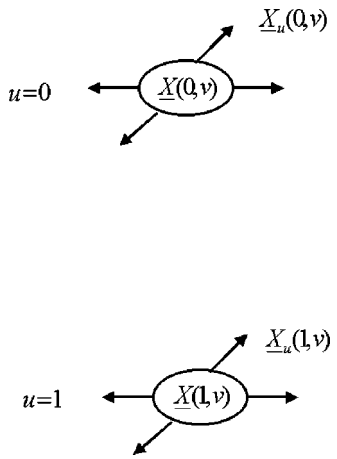

FIG. 1. Boundary conditions for a single-patch vesicle.

In the next section we shall illustrate how the method may be applied to the present problem by parametrizing a simple vesicle shape and showing how the parameters may be chosen in order to obtain the shape with a locally minimum energy.

III. SIMPLE PARAMETRIZATION OF A VESICLE SHAPE

In this section we will use a periodic solution to Eq. (2) to parametrize the shape of a vesicle in terms of a single periodic surface patch. We take the boundary curves $\underline{X}(0,v)$ and $\underline{X}(1,v)$ to be points (degenerate curves) at the ''poles'' of the vesicle, and use the derivative boundary conditions on $\underline{X}_u(0,v)$, $\underline{X}_u(1,v)$, $\underline{X}_{uu}(0,v)$, $\underline{X}_{uu}(1,v)$ to produce an appropriate shape for the surface. The boundary conditions are illustrated in Fig. 1. The function boundary conditions are shown as closed curves of finite size, whereas in reality they are points (or at least very small). The first-derivative boundary conditions are shown as vector fields distributed around the boundary curves. Note that the magnitude and direction of the vectors $\underline{X}_u(0,v)$, $\underline{X}_u(1,v)$ can vary around the boundaries. The first derivative boundary conditions have an intuitive effect on the shape, forcing the surface away from the boundaries in a particular direction. Note that care should be taken in the choice of the first derivative conditions to ensure that the surface normal is continuous at the poles. The boundary conditions on the second derivatives $\underline{X}_{uu}(0,v)$, $\underline{X}_{uu}(1,v)$ can be represented in a similar way as vector fields distributed around the boundaries, but for the sake of clarity they have been omitted from Fig. 1.

Being periodic, the boundary conditions can be expressed as Fourier series

$$\underline{f}^0(v)=\underline{C}^0_0+\sum_{n=1}^{M}\{\underline{C}^0_n\cos(nv)+\underline{S}^0_n\sin(nv)\}, \quad (6a)$$

$$\underline{f}^1(v)=\underline{C}^1_0+\sum_{n=1}^{M}\{\underline{C}^1_n\cos(nv)+\underline{S}^1_n\sin(nv)\}, \quad (6b)$$

$$\underline{f}^0_u(v)=\underline{C}^0_{u,0}+\sum_{n=1}^{M}\{\underline{C}^0_{u,n}\cos(nv)+\underline{S}^0_{u,n}\sin(nv)\}, \quad (6c)$$

$$\underline{f}^1_u(v)=\underline{C}^1_{u,0}+\sum_{n=1}^{M}\{\underline{C}^1_{u,n}\cos(nv)+\underline{S}^1_{u,n}\sin(nv)\}, \quad (6d)$$

$$\underline{f}^0_{uu}(v)=\underline{C}^0_{uu,0}+\sum_{n=1}^{M}\{\underline{C}^0_{uu,n}\cos(nv)+\underline{S}^0_{uu,n}\sin(nv)\}, \quad (6e)$$

$$\underline{f}^1_{uu}(v)=\underline{C}^1_{uu,0}+\sum_{n=1}^{M}\{\underline{C}^1_{uu,n}\cos(nv)+\underline{S}^1_{uu,n}\sin(nv)\}, \quad (6f)$$

where M is finite by choice, and the $\underline{C}^0_0$, $\underline{C}^0_n$, $\underline{S}^0_n$, etc. are constant vectors. Expressing the boundary conditions in this way allows the solution for the surface to be readily obtained in closed form. As mentioned above, a method has been devised for obtaining the solution in closed form for general periodic boundary conditions [23]. However, in the present work, restricting the boundary conditions to a finite Fourier series does not appear to restrict the range of surface shapes that can be obtained. The Fourier coefficients $\underline{C}^0_n$, $\underline{S}^0_n$ etc., along with the smoothing parameter a, form the shape variables p_i that control the shape of the vesicle surface. In fact, many of these parameters are zero and fixed during the optimization that takes place to find the shape of minimum energy. So, for example, in the results described below, the boundary curves are taken to be points which can only move along a single axis (the z axis), so consequently the only nonzero Fourier coefficients for the function boundary conditions (6a) and (6b) are the zeroth-order z coefficients. Furthermore, the zeroth-order coefficients for the first derivative boundary conditions (6c) and (6d) are taken to be zero, since otherwise a singular surface would be produced at the poles.

An example shape is shown in Fig. 2(a) for which the nonzero Fourier coefficients are given in Table I. The effect of changing some of the shape parameters is shown in Figs. 2(b)–2(d). In Fig. 2(b) the z separation of the two boundary curves has been increased; in Fig. 2(c) the magnitude of the first derivative boundary conditions has been increased, forcing the surface outwards away from the boundaries; while in Fig. 2(d) the value of the smoothing parameter has been increased. Thus it can be seen that the effect of these parameters upon the surface shape has a straight forward geometric effect.

The surfaces shown in Fig. 2 have been produced by generating a quadrilateral mesh on the surface from a rectangular mesh in (u,v) parameter space, and this mesh is then rendered as a shaded surface using standard computer graphics techniques. Although each surface patch is infinitely differentiable within its interior, some of the computer images have a curve running along their surface across which there appears to be a discontinuous change in the direction of the surface normal. This curve corresponds to $v=0,2\pi$ and the apparent jump in the surface normal is an artifact of the shading algorithm.

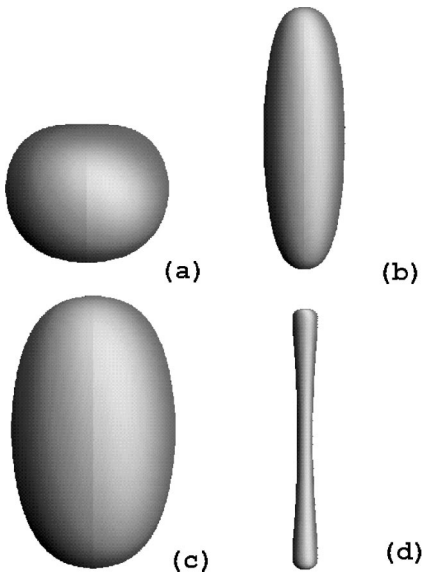

FIG. 2. The effect of boundary conditions and smoothing parameter upon vesicle shape.

Note that having a closed-form expression for the solution means that the surfaces can be generated in a fraction of a second, and that the surface properties such as curvature can be calculated explicitly at all points on the surface as a function of u and v.

A. Surface optimization

As mentioned above, the SC model for surface energy is used in this paper (with the exception of some results for the ADE model given in Sec. V A), so that the surface energy of the vesicle is given by a surface integral of the form

$$W[S]=\frac{\kappa}{2}\int dA(C_1+C_2-C_0)^2+\frac{\kappa_G}{2}\int dA(C_1C_2), \quad (7)$$

where C_1 and C_2 are the principal curvatures, C_0 is the spontaneous curvature, dA is an element of surface, and S denotes the shape of the object. The value of the surface energy W will change as the shape changes in response to changes in the values of shape parameters $(p_1,p_2,\ldots,p_n)$,

TABLE I. Nonzero shape parameters for Fig. 2(a); smoothing parameter=1.

Fourier coefficient	x component	y component	z component
$\underline{C}^1_0$	0	0	1.5
$\underline{C}^0_{u,1}$	3	0	0
$\underline{C}^1_{u,1}$	−3	0	0
$\underline{S}^0_{u,1}$	0	3	0
$\underline{S}^1_{u,1}$	0	−3	0

so that W is a function of the shape parameters $W(p)$ where $p=(p_1,p_2,\ldots,p_n)$. Although the surface is given in closed form, which allows the values of the the principal curvatures and the Jacobian relating an element of area in parameter space $dudv$ to the corresponding area element dA on the surface to be calculated exactly, the value of W must be estimated numerically and here this was done using the trapezium or Simpson's rule. Note that the boundary conditions are such that at the poles the surface curvature is continuous so that, as the vesicle has constant topological genus, the last term in Eq. (7) is ignored during the surface optimization.

The next step is to select values for the shape parameters such that the surface energy of the vesicle is minimized. This is done automatically using a technique for numerical minimization, of which there are many to choose. The particular method used for this work was an implementation of the well-known Broyden-Fletcher-Goldfarb-Shanno (BFGS) algorithm. BFGS is a quasi-Newton method and uses successive line minimizations in parameter space to find a (local) minimum in the objective function, which in this case consists of the surface energy plus constraint terms. The search directions are calculated from the gradient of the objective function in parameter space, and here these gradients were calculated by using second-order finite differences. For a quadratic objective function of N variables, the BFGS algorithm will find the function minimum using no more than N line minimizations. In the present application, the objective function is more complicated than quadratic, and there exists more multiple local minima. The details of the BFGS algorithm are extensively documented; however, one particularly useful description from a practical point of view is given in Press *et al.* [26].

The optimization is carried out subject to the constraints of constant surface area and constant enclosed volume. The constraint of constant area arises due to the strong hydrophobic effect of the hydrophobic tail which means that individual molecules will not leave the bilayer in order to enter solution; the constraint of constant volume arises from the condition that no osmotic pressure builds up across the bilayer. These two constraints are justified in more detail in [1]. The constraints were imposed using the method of Lagrange multipliers (see, for example, [27]), so that the objective function used in the optimization was of the form

$$W[S]=\frac{\kappa}{2}\int dA(C_1+C_2-C_0)^2+P\int dV+\lambda\int dA, \tag{8}$$

where dV is an element of the volume V enclosed by the vesicle, and P and λ are Lagrange multipliers.

The optimization is started at some point in parameter space. Due to the nonlinear nature of the problem, the objective function has more than one local minimum in parameter space, and therefore the optimization can find different (stable) stationary states depending on where the optimization is started. In the results described below, the method is used to find the surface energy as a function of the relevant dimensionless control parameters such as reduced volume. This was achieved by beginning the optimization at a particular point in parameter space, finding a stationary state for a given value of the control parameter, then starting a new optimization for a new value of the parameter using the previously found stationary state as the starting point for the new optimization. If the two values of the control parameters are close, then the stationary vesicle configuration found by the new optimization will often, but not necessarily, be on the same branch as the previous one. This process is then repeated and so the given branch on the phase diagram can be mapped out.

B. Phase diagram for zero spontaneous curvature

For the SC model, due to the scale invariance of the surface energy, the phase diagram for axisymmetric shapes depends only on two dimensionless control parameters, the reduced volume given by

$$v\equiv V/\left(\frac{4\pi}{3}R_0^3\right), \tag{9}$$

where

$$R_0\equiv\sqrt{4\pi A_0}, \tag{10}$$

where A_0 is the surface area of the vesicle, and the reduced spontaneous curvature c_0 is given by

$$c_0\equiv C_0R_0. \tag{11}$$

.

In this section we will concentrate upon vesicles having zero spontaneous curvature in order to validate the method against previously obtained results. The shape parameters that were allowed to vary in the optimization were the smoothing parameter a, and the following Fourier coefficients: $(\underline{C}_0^1)_z$, $\underline{C}_{uu,0}^1$, $\underline{C}_{uu,0}^0$, $(\underline{C}_{u,n}^1)_x$, $(\underline{C}_{u,n}^1)_y$, $(\underline{C}_{u,n}^0)_x$, $(\underline{C}_{u,n}^0)_y$, $(\underline{S}_{u,n}^1)_x$, $(\underline{S}_{u,n}^1)_y$, $(\underline{S}_{u,n}^0)_x$, $(\underline{S}_{u,n}^0)_y$, $\underline{C}_{uu,n}^1$, $\underline{C}_{uu,n}^0$, $\underline{S}_{uu,n}^1$, $\underline{S}_{uu,n}^0$, where $n\leq M$. Thus, during the optimization the shape of the vesicle could be changed by varying the smoothing parameter, the length of its axis, the curvature at the poles, and the length of the vectors $\underline{X}_u(0,v)$ and $\underline{X}_u(1,v)$ at the poles. Note, however, that the surface normal at the poles remains continuous and parallel to the z axis.

In the initial choice of parametrization it is advisable to keep the number of shape parameters as low as possible in order to reduce the computational cost of optimization. If the model needs to be refined at a later stage, in order to produce localized features in the geometry, for example, a hierarchical approach can be adopted by adding higher-order Fourier modes gradually or by adding more surface patches (see [22]). Here, to keep down the cost of the optimization, the maximum mode number M was set at one. However, besides the results described below, simulations were carried out with $M=4$ in order to test the code. The presence of these higher-order modes would allow nonaxisymmetric shapes to appear if they represented a state of minimal energy. Nevertheless, the optimization returned axisymmetric shapes, setting the amplitude of the higher modes effectively to zero.

The results are presented in Fig. 3 which gives the phase diagram calculated for $c_0=0$. The results show the surface energy in units of $8\pi\kappa$ as a function of reduced volume for both the oblate and prolate branches. The prolate branch was found by taking a long and thin, but otherwise arbitrary, ellipsoid for the starting shape, whilst the oblate branch was

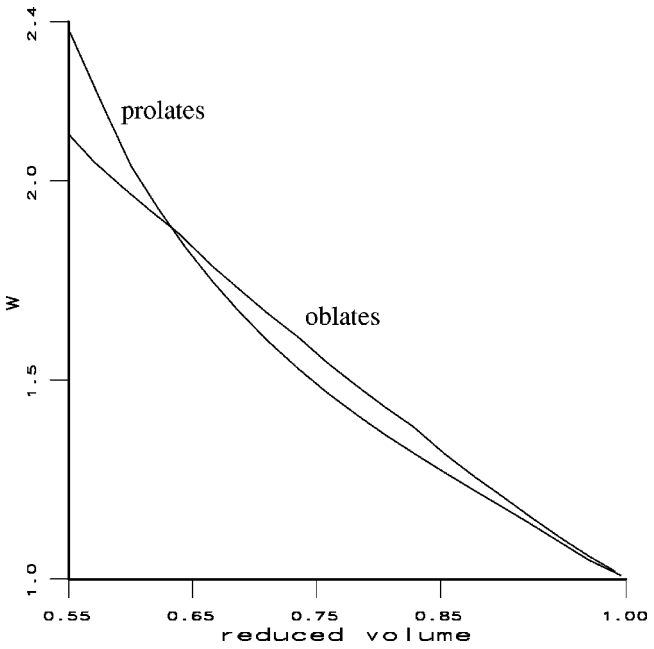

FIG. 3. Phase diagram for an axisymmetric, single-patch vesicle ($C_0=0$).

found by taking an arbitrary squat ellipsoid for the starting shape. Both optimizations used a starting reduced volume v of 0.55 and then, after a stationary shape had been found, started again with an increased reduced volume (using the previous found stationary shape as the starting point), and so on, until a value of $v=1.0$ had been reached. Figure 4 shows some representative shapes. Figures 4(a) and 4(b) show two shapes from the prolate branch with reduced volumes of 0.55 and 0.758 respectively; Figs. 4(c) and 4(d) show two shapes from the oblate branch with reduced volumes of 0.55 and 0.85, respectively.

These results of Fig. 3 can be compared with those obtained by Seifert *et al.* [14] (their Fig. 8). One can see that despite the simple nature of the parametrization, there is fairly good agreement both qualitatively and quantitatively between the two sets of results. However, one feature that this simple surface model is unable to detect is the stomatocyte branch of the phase diagram. The surface model is capable of producing stomatocytelike shapes, but they are rather distorted and hence not stationary states in surface energy space. To find these it is necessary to refine the surface parametrization.

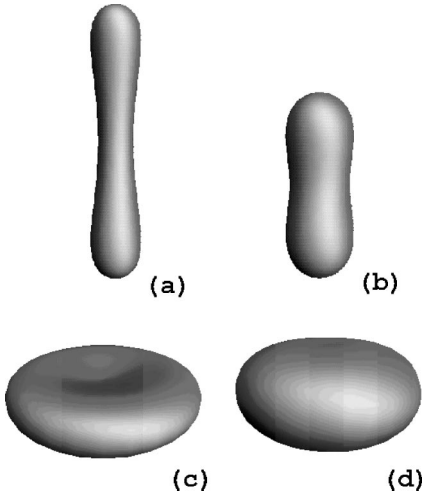

FIG. 4. Sample shapes for a single-patch vesicle ($C_0=0$): (a) $v=0.55$; (b) $v=0.758$; (c) $v=0.55$; (d) $v=0.85$.

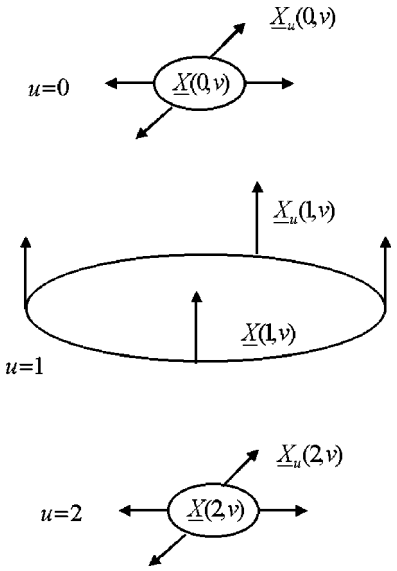

FIG. 5. Boundary conditions for two-patch vesicle parametrization.

IV. REFINED PARAMETRIZATION OF A VESICLE SHAPE

In order to increase the range of shapes that the surface model is capable finding, it is necessary to refine the parametrization by adding more surface patches, and an obvious way to do this is indicated in Fig. 5 where the boundary conditions for a surface model using two surface patches are shown. One patch forms the ''upper half'' of the vesicle and the other patch the ''lower half.'' The patches meet at a plane curve which lies in the $z=0$ plane. The other boundary for each patch is a point which is free to move along the z axis; as before the boundary conditions here are such that the tangent plane for each patch is horizontal and continuous. In Fig. 5 the boundary curves for the upper patch are labeled $u=0$ and $u=1$, while the boundary curves for the lower patch are $u=1$ and $u=2$; thus the upper patch is obtained by solving over the (u,v) domain $[0,1]\times[0,2\pi]$, while the lower patch is obtained by solving over the domain $[1,2]\times[0,2\pi]$. For obvious reasons, the $u=0$ and $u=2$ boundaries will be referred to as the poles of the surface parametrization.

At their common boundary curve, both patches meet with tangent plane and curvature continuity, which is enforced by ensuring continuity of parametric u derivatives across the boundary curve. Although parametric continuity is certainly a sufficient condition to ensure geometric continuity, it is not strictly necessary, and in principle is somewhat restrictive of the range of shapes that can be obtained. However, it is straightforward to implement and in practice does not seem to restrict the range of obtainable shape.

The shape parameters in the problem are now the Fourier coefficients of the boundary conditions imposed at the three

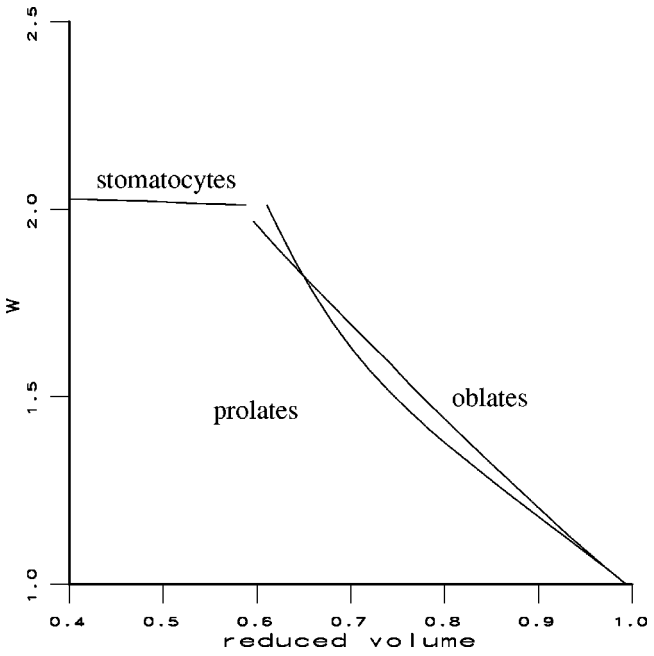

FIG. 6. Phase diagram for an axisymmetric two-patch vesicle ($C_0=0$).

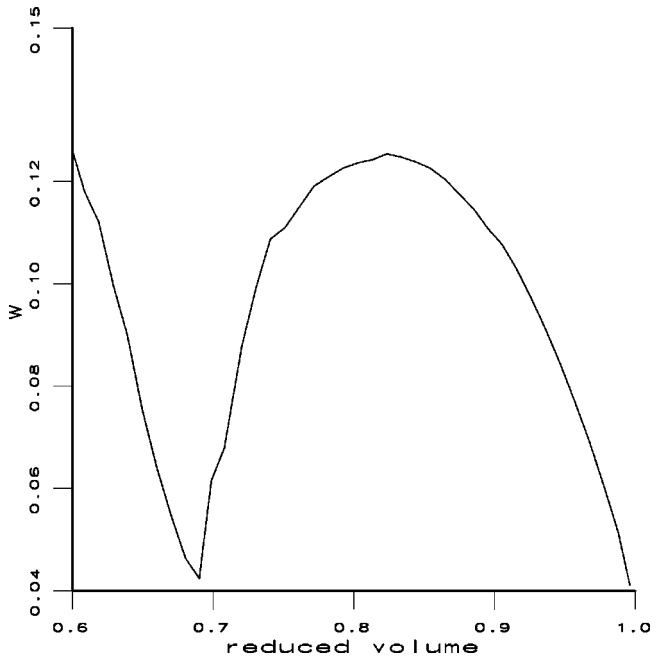

FIG. 8. Phase diagram for an axisymmetric two-patch vesicle with $C_0=2.4$.

boundary curves, subject to the following constraints which reduce the number of Fourier coefficients that are allowed to vary in the optimization: (a) the $u=0$ and $u=2$ boundaries can only move along the z axis; (b) at the poles the surface's tangent plane remains parallel to the (x,y) plane; (c) there is continuity of parametric derivatives across the $u=1$ curve.

A. Phase diagram for zero spontaneous curvature

In this section the optimizations of Sec. III B are repeated using the refined surface parametrization. The resulting phase diagram is shown in Fig. 6 with surface energy given in units of $8\pi\kappa$, and some representative shapes are shown in Fig. 7. Now it is possible to find not only the prolate and oblate branches, but also the stomatocyte branch. Figure 7(a) shows a prolate with $v=0.6$; Fig. 7(b) shows an oblate with $v=0.6$; while Fig. 7(c) shows a stomatocyte with $v=0.39$. By comparing the phase diagram Fig. 6 with that obtained by Seifert *et al.* [14], one can see that the surface model is able to to represent the states of minimum energy quite accurately. Note that like the prolate and oblate branches the stomatocyte branch was found by using a starting shape qualitatively similar to the shapes one was trying to detect, so that in the case of the stomatocyte branch this was a shape that was slightly ''cup-shaped.'' Note also that in the optimization the value of the maximum Fourier mode M number was limited to 1.

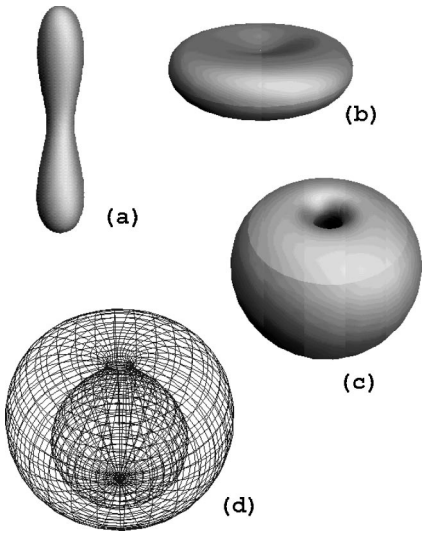

FIG. 7. Sample shapes for a two-patch vesicle ($C_0=0$): (a) prolate: $v=0.6$; (b) oblate: $v=0.6$; (c) stomatocyte: $v=0.39$.

B. Phase diagram for $c_0=2.4$

As a further test of the shape parametrization, the value of the reduced spontaneous curvature was set to 2.4 and another sequence of optimizations was run, this time starting from a reduced volume of $v=1$. This was done in order to compare the results with Seifert *et al.* [14] (cf. their Fig. 11). The phase diagram for the present calculations is shown in Fig. 8 which plots surface energy in units of $8\pi\kappa$ against reduced volume; some representative shapes are shown in Fig. 9. The shape in Fig. 9(a) has a reduced volume of 0.751; the shape in Fig. 9(b) has a reduced volume of 0.72; the shape in Fig. 9(c) has a reduced volume of 0.68; and the shape in Fig. 9(d) has a reduced volume of 0.6.

Comparing these results with those of Seifert *et al.* [14], show that the method has found the states of lowest energy in the following ranges of reduced volumes: $v=1\rightarrow v\approx 0.72$ (prolates); $v\approx 0.72\rightarrow v\approx 0.69$ (pears); $v\approx 0.69\rightarrow v=0.6$ (prolates). Note that these branches apparently correspond to Seifert *et al.* prolates-1, C_1^{pear}, and prolate-2 branches, respectively. The reason why shapes from the C^{pear} branch are not detected, despite having lower energies than shapes on the C_1^{pear} branch, is probably due to the fact that the limits set on the permissable parameter variation in

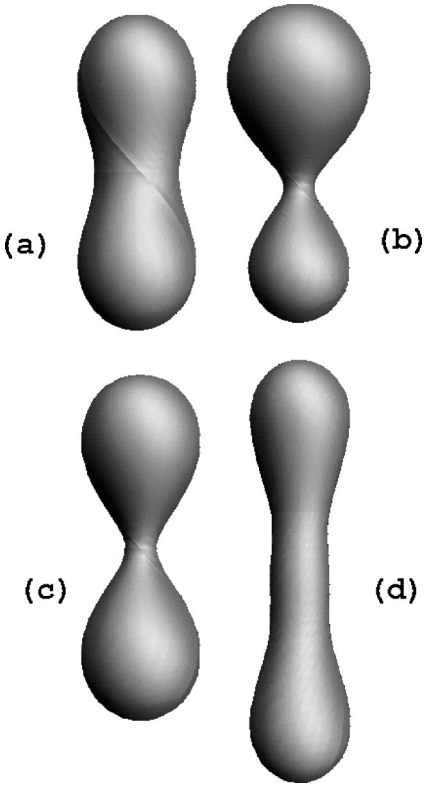

FIG. 9. Sample shapes for an axisymmetric vesicle with $C_0 = 2.4$: (a) $v = 0.751$; (b) $v = 0.72$; (c) $v = 0.68$; (d) $v = 0.6$.

the optimization routine did not allow the type of shapes with very thin ''necks'' that occur on the C^{pear} branch.

C. Phase diagram for $c_0 = 3.0$

This section gives presents results for axisymmetric vesicles for which $c_0 = 3.0$. The phase diagram for the present calculations is shown in Fig. 10 which plots surface

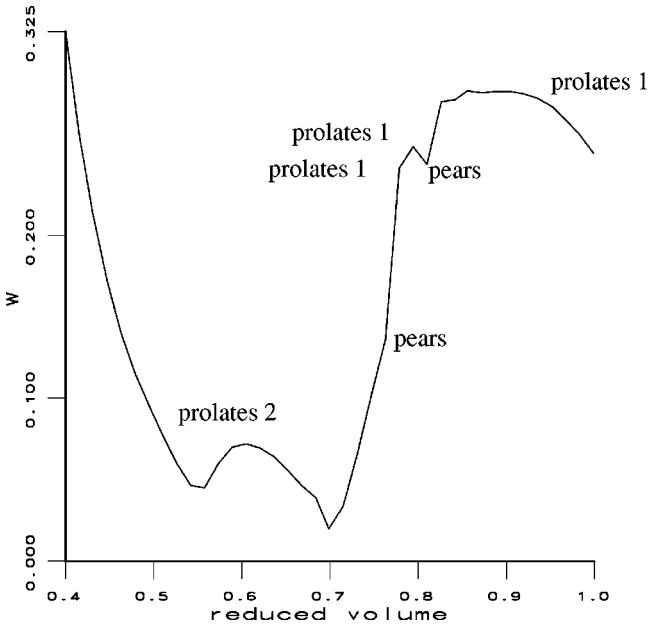

FIG. 10. Phase diagram for an axisymmetric vescile with $C_0 = 3.0$.

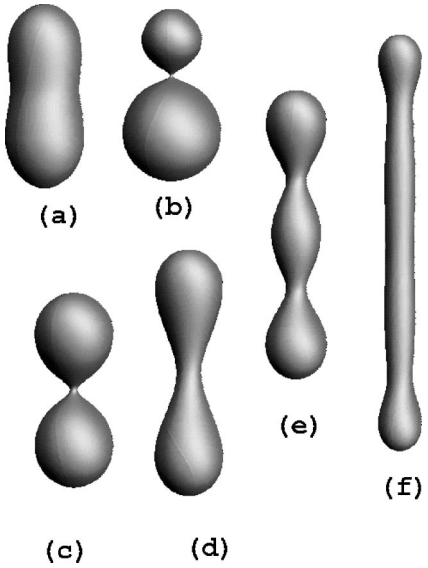

FIG. 11. Sample shapes for an axisymmetric vesicle with $C_0 = 3.0$: (a) $v = 0.826$; (b) $v = 0.763$; (c) $v = 0.698$; (d) $v = 0.652$; (e) $v = 0.541$; (f) $v = 0.4$.

energy in units of $8\pi\kappa$ against reduced volume; some representative shapes are shown in Fig. 11. The shape in Fig. 11(a) has a reduced volume of 0.826; the shape in Fig. 11(b) has a reduced volume of 0.763; the shape in Fig. 11(c) has a reduced volume of 0.698; the shape in Fig. 11(d) has a reduced volume of 0.652; the shape in Fig. 11(e) has a reduced volume of 0.541; and the the shape in Fig. 11(f) has a reduced volume of 0.4. Comparison with the results of Seifert *et al.* [14] show that the method has detected the states of lowest energy in the range of reduced volumes $v = 1. \rightarrow v = 0.4$; namely the prolates-1, pears, and prolates-2. Note that near to the crossing point of the prolates-1 branch and the lower of the pear branches at $v \approx 0.82$, the stable states found by successive optimizations jump between the two branches. This is due to the fact that the optimization algorithm, in searching for an energy minimum in parameter space does so by taking a finite step in its chosen search direction. Thus when two branches are close in energy the optimization algorithm is affected by numerical noise in the estimate of the search direction and is liable to end up on either branch. Also note that in the region $v \approx 0.748 \rightarrow v \approx 0.707$, some stationary pear shapes are obtained whereas one would expect no stable pears to exist [14]. The probable reason for this is that there are finite parameter bounds set on the curvature boundary conditions that prevent the geometry at the neck from becoming too extreme, the effect of which is to stabilize shapes in this region. Nevertheless, elsewhere in the phase diagram the method is able to represent accurately the expected stable shapes.

V. NONAXISYMMETRIC VESICLE SHAPES

The previous results have been confined to relatively simple stationary states by limiting the Fourier mode number varied in the optimization to $M = 1$ (except to test the optimization). Most previous work on vesicle configurations has concentrated upon axisymmetric shapes, but there have been observations and simulations of nonaxisymmetric shapes

(e.g., [28,29,15–17]). Numerical simulations of such shapes have usually been carried out through the procedure of minimizing the curvature energy of a triangulated surface approximation to the vesicle, e.g., [17,18], (although other methods have been used, e.g., [16,29,15]). The triangulated surface approach is computationally very expensive since the number of shape parameters that must be varied in the energy minimization is effectively the number of surface grid points, which is typically a few thousand. However, nonaxisymmetric shapes can be obtained using the parameterization method described above, certainly by increasing the number of Fourier modes that are varied in the optimization so that $M>1$, but also in principle for the case $M=1$. Of course, whether or not these nonaxisymmetric shapes are stationary depends on the model for the surface energy. The important point is that the present method can represent nonaxisymmetric shapes using a much smaller set of design variables (by an order of magnitude), which greatly reduces the computational expense of numerical optimization. In the results presented next, the nonaxisymmetric shapes were found as a result of optimizations run, in a few hours on a UNIX workstation, or overnight on a fast PC, although the timing depends on the accuracy required. Note that to find a nonaxisymmetric branch it was sometimes necessary to use a nonaxisymmetric starting shape.

A. ADE model

In this section we show some results obtained using the area-difference-elasticity (ADE) model and compare them with those obtained by Jarić *et al.* [16]. The surface energy $W[S]$ in the ADE model is given by an expression of the form [1]

$$W[S]\equiv\frac{\kappa}{2}\int dA(C_1+C_2-C_0)^2+\frac{\overline{\kappa}}{2}\frac{\pi}{AD^2}(\Delta A[S]-\Delta A_0)^2. \tag{12}$$

Like the spontaneous curvature model the first term represents the local bending energy, whereas the second term represents the cost in elastic energy of causing the area difference between the inner and outer layers of the membrane

$$\Delta A[S]=2D\oint dAH \tag{13}$$

(where H is the local mean curvature $[\frac{1}{2}(C_1+C_2)]$), to deviate from the ''relaxed'' value ΔA_0 [16]; $\overline{\kappa}$ is the nonlocal bending modulus and D is the thickness of the bilayer. Following Jarić *et al.* [16] the area difference and relaxed area difference can be nondimensionalized thus

$$m[S]\equiv\frac{\Delta A}{2DR_0} \tag{14}$$

and

$$m_0\equiv\frac{\Delta A_0}{2DR_0} \tag{15}$$

so that the surface energy may then be written in the following convenient form:

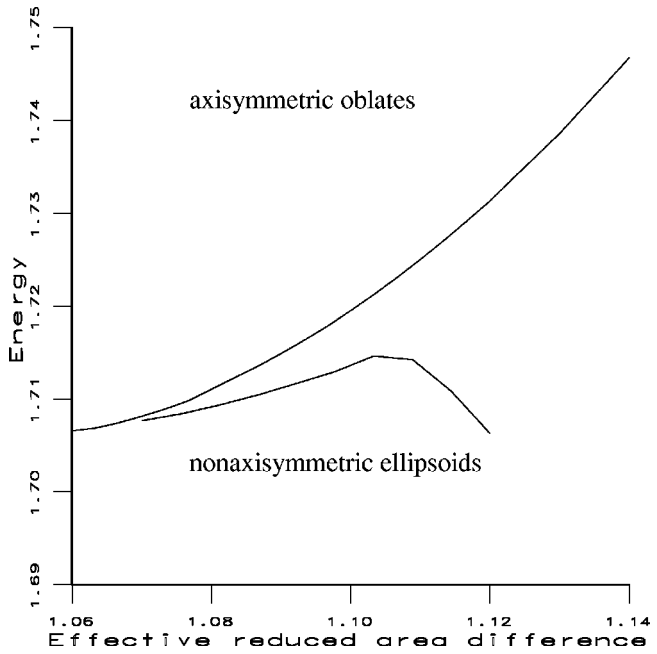

FIG. 12. Energy W as a function of the area difference $\overline{m}_0$ for an ADE model at $v=0.7$.

$$W[S]\equiv\kappa\left(\tfrac{1}{2}\int dA(2H)^2+\alpha(m[S]-\overline{m}_0)^2+w_0\right) \tag{16}$$

where $\alpha\equiv\overline{\kappa}/\kappa$, w_0 is a constant and

$$\overline{m}_0\equiv m_0+\frac{2c_0}{\alpha}. \tag{17}$$

Thus, to change from the SC model to the ADE model it is a simple matter to replace the energy functional in Eq. (8) with the energy functional of Eq. (16) (whilst retaining the constraints on area and volume). The relevant control parameters are now $\overline{m}_0$ and v. Jaric *et al.* [16] describe the various locally stable branches of the phase diagram of this model which in the main consist of axisymmetric shapes, i.e., oblate and prolate ellipsoids, pears, and stomatocytes. However, they also find, in relatively small regions of the phase plane, regions where locally stable nonaxisymmetric shapes exist.

Figure 12 presents a plot of energy W against effective reduced area difference $\overline{m}_0$ for a fixed value of v at $\alpha=1.4$ in a region where locally stable nonaxisymmetric shapes exist. Two branches are shown: the axisymmetric oblates and the nonaxisymmetric ellipsoids which bifurcate from them just below $\overline{m}_0/4\pi=1.08$. Figure 13 shows a representative shape from the oblate branch (cf. the shapes found by Heinrich *et al.* [15]). Each branch has been calculated using the

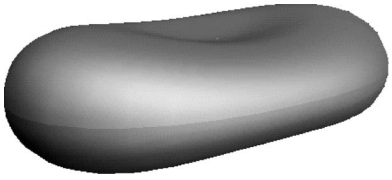

FIG. 13. A representative nonaxisymmetric ellipsoid for ADE results shown in Fig. 12: $v=0.7$; $\overline{m}_0=1.09$.

method described in this paper. Note that if the nonaxisymmetric branch is followed beyond $\bar{m}_0/4\pi$ about 1.11, the calculated shapes jump to the prolate branch. In the numerical calculation of the nonaxisymmetric branch, a value of $M=5$ was used for the number of Fourier modes in the solution. These results compare favorably with Fig. 4 of Jarić *et al.* [16], bearing in mind the fact their nonaxisymmetric shapes were calculated using brute-force energy minimization over a triangulated surface shape having 4000 grid points that represented (at the time of writing) the practical limits of their computational facilities; whereas the present results, which only have 193 free parameters, can be calculated in a few hours on a workstation or fast PC.

These results provide an illustration of the hierarchical approach in that, at first, only two modes were used in the optimization. This produced nonaxisymmetric shapes that bifurcated from the axisymmetric oblates at the correct point (just below $\bar{m}_0/4\pi=1.08$), but which were not of quite the correct shape and consequently their surface energy continued to increase monotonically with $\bar{m}_0$ (like the axisymmetric oblates). In order to refine the geometry model, the optimization was repeated using an increasing number of modes, until the case $M=5$ was found to produce a variation of energy with $\bar{m}_0$ of the correct form. The starting point for these subsequent optimizations was a nonaxisymmetric shape produced by the $M=2$ case, i.e., a starting geometry which was correct on long length scales but which required small scale refinement.

B. Starfish

As a final, rather more challenging, example of nonaxisymmetric shapes that can be calculated, some calculations of starfish vesicles are presented. It is now well established, both experimentally in the laboratory [28] and numerically [17], that under certain conditions vesicles can assume starfish shapes. Wintz *et al.* [17] present results for starfish with up to seven arms using the ADE model for the surface energy produced using a triangulated surface model with 2500 grid points. In this section we present results of calculations of starfish using the SC model for the surface energy with the value of c_0 being 1.35. The starfish shapes where calculated over a range of reduced volumes from $v=0.5$ to $v=0.33$. The maximum number of Fourier modes in the solution is $M=5$ which makes the maximum number of free parameters 193. The initial optimization was started with a fairly distorted shape having four arms (or rather bulges), although as can been seen from the representative shapes shown in Fig. 14 the stable shapes found have three arms: the shape in Fig. 14(a) has a reduced volume of 0.545; the shape in Fig. 14(b) has a reduced volume of 0.435; the shape in Fig. 14(c) has a reduced volume of 0.352; and the the shape in Fig. 14(d) has a reduced volume of 0.31. Note that not all of the shapes have a threefold mirror symmetry, although they do appear to have threefold rotational symmetry. This may be an artifact of the parametrization, in particular the number of Fourier modes used, although these results are consistent a calculation carried out with $M=6$. In fact, some of the results presented by Wintz *et al.* [17], would suggest that it is possible to find starfish shapes without any symmetry at all. Figure 15 shows a plot of surface energy against reduced volume for these shapes. The results presented in Fig. 15, which represent the stable shapes at 20 different reduced volumes, using a 61×61 surface mesh to evaluate W, can be calculated overnight on a Silicon Graphics R1000 workstation.

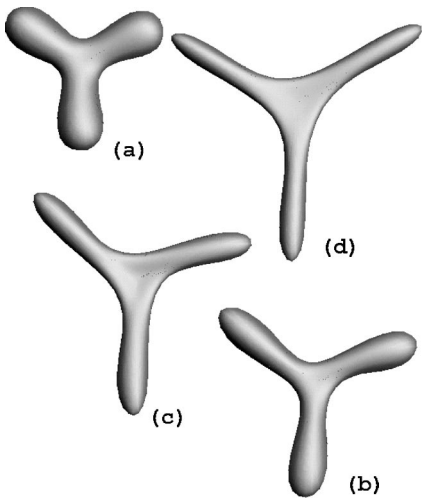

FIG. 14. Sample shapes for three-armed starfish vesicles ($C_0=1.35$): (a) $v=0.545$; (b) $v=0.435$; (c) $v=0.352$; (d) $v=0.31$.

VI. DISCUSSION

We have presented a method for producing a generic parameteric model of the shape of a vesicle which is capable of producing a wide range of shapes. Moreover, the results presented above indicate that this approach to shape parametrization, in combination with a method for numerical optimization, is capable of accurately approximating the shapes of vesicles and their surface energies. In all the cases discussed above, a hierarchical approach to the shape parametrization was adopted in which the geometry model of successively

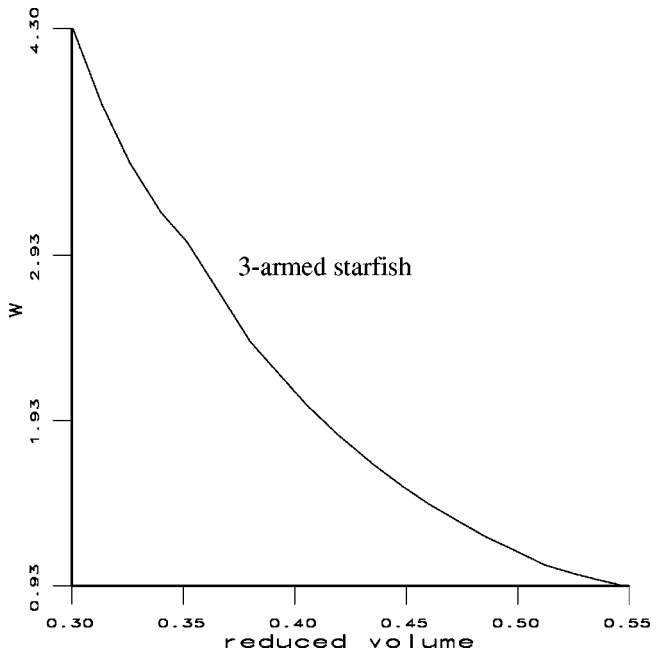

FIG. 15. Energy W as a function of the reduced volume for starfish vesicles using the SC model $C_0=1.35$.

refined to produce features on shorter and shorter length scales, by a combination of adding more surface patches and increasing the number of Fourier modes.

It is unreasonable to expect it to be as accurate or efficient as the numerical solution of the ordinary differential equation to which the shape equations reduce in the axisymmetric case. However, on the other hand, the main advantage of the method is in the nonaxisymmetric case where numerical solution of the shape equations has not proved possible for shapes that differ markedly from axisymmetry. Two examples have been used to demonstrate its ability to find nonaxisymmetric vesicle shapes: starfish vesicles in the context of the SC model and pinched dumbells in the context of the ADE model.

The ability of the method to parametrize efficiently nonaxisymmetric shapes, i.e., represent them in terms of a relatively small set of shape parameters, gives it an advantage in terms of speed over the triangulated surface approach that is most often used to find highly nonaxisymmetric shapes. In this approach, the shape parameters are effectively the coordinates of the vertices of the surface triangles of which there tends to be a large number for a complicated shape. For example, Wintz *et al.* [17] quote a figure of 2500, Jie *et al.* [18] used between 2000–3000 grid points for their simulations, while Jarić *et al.* [16] report that about 4000 grid points is the largest they could practically attempt. For the results presented in this paper, the number of free parameters is at most 193 (used in the calculations of the starfish shapes described in Sec. V B), thus such shapes can be calculated much more rapidly than by using a triangulated surface approach. Each shape parameter used in the PDE approach has a global effect on the shape of the surface, thus there are fewer parameters than for a triangulated surface model, each of whose parameters exerts only a local influence on the surrounding surface.

However, it is possible to imagine a hybrid approach in which the PDE method is used in combination with a triangulated surface model, since a surface triangulation can be obtained from the PDE description by a simple gridding in (u,v) parameter space. Thus a PDE model could be used to obtain an approximation to an optimum shape relatively rapidly, from which a triangulated surface model could be produced and used as the starting point for a brute-force optimization over the vertices to obtain a very accurate model.

This paper has only described the parametrization of shapes that are the topological equivalent of spheres, but the extension of the method to more complicated shapes, in the sense of higher genus and/or complex shape, is straightforward because shapes with handles can easily be constructed from multiple surface patches as work in the CAD area has demonstrated [30].

[1] U. Seifert, Adv. Phys. **46**, 13 (1997).
[2] Y. Bouligand, Liq. Cryst. **26**, 501 (1999).
[3] P. B. Canham, J. Theor. Biol. **26**, 61 (1970).
[4] W. Helfrich, Z. Naturforsch. C **28**, 693 (1973).
[5] E. Evans, Biophys. J. **14**, 923 (1974).
[6] S. Svetina, A. Ottova-Leitmanova, and R. Glaser, J. Theor. Biol. **94**, 13 (1982).
[7] U. Seifert, L. Miao, H. G. Döbereiner, and M. Wortis, *The Structure and Conformation of Amphiphilic Membranes*, Proceedings in Physics Vol. 66, edited by R. Lipowsky, D. Richter, and K. Kremer (Springer-Verlag, Berlin, 1992), p. 93.
[8] S. Svetina and B. Zeks, Biochim. Biophys. Acta **42**, 86 (1983).
[9] S. Svetina and B. Zeks, Eur. Biophys. J. **17**, 101 (1989).
[10] W. Wiese, W. Harbich, and W. Helfrich, J. Phys.: Condens. Matter **4**, 1647 (1992).
[11] B. Bozic, S. Svetina, B. Zeks, and R. E. Waugh, Biophys. J. **61**, 963 (1992).
[12] Z. C. Ou-Yang and W. Helfrich, Phys. Rev. A **39**, 5280 (1989).
[13] L. Miao, B. Fourcade, M. Rao, M. Wortis, and R. K. P. Zia, Phys. Rev. A **43**, 6843 (1991).
[14] U. Seifert, K. Berndl, and R. Lipowsky, Phys. Rev. A **44**, 1182 (1991).
[15] V. Heinrich, S. Svetina, and B. Zeks, Phys. Rev. E **48**(4), 3112 (1993).
[16] M. Jarić, U. Seifert, W. Wintz, and M. Wortis, Phys. Rev. E **52**, 6623 (1995).
[17] W. Wintz, H.-G. Döbereiner, and U. Seifert, Europhys. Lett. **33**, 403 (1996).
[18] Y. Jie, L. Quanhui, L. Jixing, and Z. C. Ou-Yang, Phys. Rev. E **58**, 4730 (1998).
[19] M. I. G. Bloor and M. J. Wilson, CAD **21**, 165 (1989).
[20] M. E. Mortenson, *Geometric Modelling* (Wiley, New York, 1985).
[21] C. W. Dekanski, M. I. G. Bloor, and M. J. Wilson, AIAA J. Prop. Power **13**, 398 (1997).
[22] N. E. Sevant, M. I. G. Bloor, and M. J. Wilson, *AIAA/USAF/NASA/ISSMO 7th Symposium on Multidisciplinary Analysis and Optimisaton, St. Louis, MO, September, 1998* (American Institute of Aeronautics and Astronautics, Washington, D.C., 1998), pp. 1099–1107.
[23] M. I. G. Bloor and M. J. Wilson, CAD **28**, 145 (1996).
[24] N. E. Sevant, M. I. G. Bloor, and M. J. Wilson, AIAA J. Aircraft **36(2)**, 642 (1999).
[25] T. W. Lowe, M. I. G. Bloor, and M. J. Wilson, J. Ship Res. **38**, 319 (1994).
[26] W. H. Press, B. P. Flannery, S. A. Teukolsky, and W. T. Vetterling, *Numerical Recipes: The Art of Scientific Computing (FORTRAN Version)* (Cambridge University Press, Cambridge, England, 1989).
[27] D. M. Greig, *Optimisation* (Longman, New York, 1980).
[28] H. Hotani, J. Mol. Biol. **178**, 113 (1984).
[29] V. Heinrich, M. Brumen, R. Heinrich, S. Svetina, and B. Zeks, J. Phys. II **2**, 1081 (1992).
[30] C. W. Dekanski, M. I. G. Bloor, and M. J. Wilson, Comput. Methods Appl. Mech. Eng. **137**, 411 (1996).